*Anal. Chem.* **2005,** *77,* 6243−6249

# Protein Capture in Silica Nanotube Membrane 3-D Microwell Arrays

**Myungchan Kang, Lacramioara Trofin, Miguel O. Mota, and Charles R. Martin***

*Department of Chemistry and Center for Research at the Bio/Nano Interface, University of Florida, Gainesville, Florida 32611-7200*

**The microarray format has allowed for rapid and sensitive detection of thousands of analyte DNAs in a single sample, and there is considerable interest in extending this technology to protein biosensing. While glass is the most common substrate for microarrays, its binding capacity is limited because the glass surface is flat. One way to overcome this limitation is to develop arrays based on porous materials. Such "3-D" arrays can provide greater sensitivity because both the capture molecules and the analyte species they bind are immobilized throughout the thickness of the porous material. We describe here 3-D protein microarrays based on nanopore alumina membranes that contain silica nanotubes within the pores. These microarrays are prepared via a plasma-etch method using a TEM grid as the etch mask and consist of individual nanotube-containing microwells imbedded in a Ag film that coats the alumina membrane surface. We show that the microwells can be functionalized with antibodies and that these antibodies can capture their antigen proteins, which serve as prototype analytes. The analyte proteins are fluorescently tagged, which allows for fluorescence microscopy-based imaging of the array. The Ag surrounding the microwells shows very low background fluorescence, thus improving the signal-background ratio obtained from these arrays.**

The microarray format has allowed for rapid and sensitive detection of thousands of analyte DNAs in a single sample,[1−3] and there is considerable interest in extending this technology to protein biosensing.[4−15] In the microarray format, molecules that capture the analyte species are spotted in an array pattern across a substrate surface. While glass is the most common substrate for microarrays,[3] its binding capacity is limited because the glass surface is flat. One way to overcome this limitation is to develop arrays based on porous materials.[4,6,11,16−19] Such "3-D" arrays can provide greater sensitivity because both the capture molecules and the analyte species they bind are immobilized throughout the thickness of the porous material.

3-D supports should be especially advantageous for protein microarrays. This is because the enhanced binding capacity of the 3-D system provides broad dynamic range of detection, and this is essential because the concentrations of the protein analytes in the sample may vary by up to 10 orders of magnitude.[12,20−22] A broader dynamic range is possible with the 3-D system because the enhanced surface area available for analyte binding (relative to a 2-D system) means that saturation of the device occurs at higher analyte concentrations than with an analogous 2-D system. Furthermore, unlike DNA, there is no simple method to amplify the concentrations of protein analytes. In addition, the water retained within the pores of a porous substrate minimizes the chance of drying-induced denaturation of protein analytes.[18]

A number of different materials have been used to make 3-D protein arrays including nitrocellulose,[6,16] poly(vinylidene difluoride),[17] polyacrylamide gel pads,[18] agarose films,[4] poly(dimethysiloxane) nanowells,[19] and porous silicon.[11] However, problems such as limited spot density, high background (e.g., fluorescence) signal, and long washing times are often observed.[14] For these reasons, there is considerable interest in developing new generations of 3-D array-sensing platforms. For example, it has recently been shown that nanopore alumina membranes can be used as

* Corresponding author: (e-mail) crmartin@chem.ufl.edu.

(1) Schena, M.; Shalon, D.; Davis, R. W.; Brown, P. O. *Science* **1995**, *270*, 467−470.
(2) DeRisi, J. L.; Iyer, V. R.; Brown, P. O. *Science* **1997**, *278*, 680−686.
(3) Schena, M. *Microarray analysis*, 1st ed.; J. Wiley: Hoboken, NJ, 2003.
(4) Afanassiev, V.; Hanemann, V.; Wolfl, S. *Nucleic Acids Res.* **2000**, *28*, e66ii−v.
(5) Cahill, D. J. *J. Immunol. Methods* **2001**, *250*, 81−91.
(6) Ge, H. *Nucleic Acids Res.* **2000**, *28*, e3.
(7) Huang, R. P. *J. Immunol. Methods* **2001**, *255*, 1−13.
(8) Lueking, A.; Konthur, Z.; Eickhoff, H.; Bussow, K.; Lehrach, H.; Cahill, D. J. *Curr. Genet.* **2001**, *2*, 151−159.
(9) MacBeath, G.; Koehler, A. N.; Schreiber, S. L. *J. Am. Chem. Soc.* **1999**, *121*, 7967−7968.
(10) MacBeath, G.; Schreiber, S. L. *Science* **2000**, *289*, 1760−1763.
(11) Ressine, A.; Ekstrom, S.; Marko-Varga, G.; Laurell, T. *Anal. Chem.* **2003**, *75*, 6968−6974.
(12) Templin, M. F.; Stoll, D.; Schwenk, J. M.; Poetz, O.; Kramer, S.; Joos, T. O. *Proteomics* **2003**, *3*, 2155−2166.
(13) Zhu, H.; Snyder, M. *Curr. Opin. Chem. Biol.* **2001**, *5*, 40−45.
(14) Zhu, H.; Snyder, M. *Curr. Opin. Chem. Biol.* **2003**, *7*, 55−63.
(15) Espina, V.; Mehta, A. I.; Winters, M. E.; Calvert, V.; Wulfkuhle, J.; Petricoin, E. F., III; Liotta, L. A. *Proteomics* **2003**, *3*, 2091−2100.
(16) Joos, T. O.; Schrenk, M.; Hopfl, P.; Kroger, K.; Chowdhury, U.; Stoll, D.; Schorner, D.; Durr, M.; Herick, K.; Rupp, S.; Sohn, K.; Hammerle, H. *Electrophoresis* **2000**, *21*, 2641−2650.
(17) Walter, G.; Bussow, K.; Cahill, D.; Lueking, A.; Lehrach, H. *Curr. Opin. Microbiol.* **2000**, *3*, 298−302.
(18) Arenkov, P.; Kukhtin, A.; Gemmell, A.; Voloshchuk, S.; Chupeeva, V.; Mirzabekov, A. *Anal. Biochem.* **2000**, *278*, 123−131.
(19) Zhu, H.; Klemic, J. F.; Chang, S.; Bertone, P.; Casamayor, A.; Klemic, K. G.; Smith, D.; Gerstein, M.; Reed, M. A.; Snyder, M. *Nat. Genet.* **2000**, *26*, 283−289.
(20) Celis, J. E.; Gromov, P. *Cancer Cell* **2003**, *3*, 9−15.
(21) Hunter, T. *Cell* **2000**, *100*, 113−127.
(22) Jeong, H.; Tombor, B.; Albert, R.; Oltvai, Z. N.; Barabasi, A. L. *Nature* **2000**, *407*, 651−654.

10.1021/ac0508907 CCC: $30.25 
Published on Web 09/10/2005

3-D supports for gene arrays.[23,24] In this case, capture DNA species were simply spotted in an array pattern across the nanopore alumina surface.

We have been investigating the use of such nanopore alumina membranes as supports for array-based protein sensing. We have prepared 3-D protein microarrays based on nanopore alumina that contains silica nanotubes within the pores. These microarrays are prepared via a plasma-etch method using a transmission electron microscopy (TEM) grid as the etch mask and consist of individual nanotube-containing microwells imbedded in a Ag film that coats the membrane surface. The microwells were functionalized with antibodies, and these antibodies captured their antigen proteins, which served as prototype analytes. The analyte proteins were fluorescently tagged, which allowed for fluorescence microscopy-based imaging of the array. The Ag surrounding the microwells showed low background fluorescence, thus improving the signal-background ratio obtained from these arrays. Furthermore, the extent of functionalization is higher for the silica nanotube membrane than for the membrane without these nanotubes. The results of these investigations are reported here.

## EXPERIMENTAL SECTION

**Materials.** Aluminum foil (99.9998%) and silver wire were obtained from Alfa Aesar, and microscope premium finest glass slides were obtained from Fisher. (3-Aminopropyl)trimethoxysilane (APTS; Gelest), triethoxysilylbutyl aldehyde (Gelest), tetraethyl orthosilicate (Aldrich), rhodamine B isothiocyanate (Aldrich), human and mouse IgG (Sigma-Aldrich), anti-human IgG labeled with Alexa 488 fluorophore (Molecular Probes), and anti-mouse IgG labeled with Alexa 594 fluorophore (Moecular Probes) were used as received.

A spin-coating cresol Novolak polymer solution (FSC-M, Shipley) and a solvent system to remove the spin-coated polymer (remover 1165, Shipley) were obtained from MicroChem. Silver plating solution (Ag 1025) was obtained from Technic. TEM copper grids (400 mesh, Pelco) were purchased from Ted Pella. The nanopore alumina membranes were either prepared in-house or obtained commercially (nominally 200-nm-diameter pores, 60 $\mu$m thick, Whatman). The in-house membranes were prepared by electrochemically oxidation of aluminum using the two-step anodization method.[25,26] Briefly, the Al foils were first electropolished at 15 V for 10 min at 70 °C in a solution that was 95 wt % $H_3PO_4$, 5 wt % $H_2SO_4$, and 0.2 M $CrO_3$. The cathode was a Pb plate.

After rinsing with purified water, the polished Al foil was anodized at 50 V in 5 wt % aqueous oxalic acid at 0 °C for 15 h. The cathode was a stainless steel plate. This resulted in the formation of a precursor nanopore alumina film on the surface of the Al foil. This precursor film was dissolved away in an aqueous solution that was 0.2 M $CrO_3$ and 0.4 M $H_3PO_4$, at 70 °C. As discussed by Masuda and Satoh, this dissolution step leaves a highly ordered pattern of scallops on the Al substrate.[25]

In the second step, this textured Al substrate was anodized at 50 V in the 5 wt % oxalic acid solution. This voltage yields membranes with pore diameter of ~80 nm, as determined by field emission scanning electron microscopy. The anodization time was varied in order to vary the thickness of the alumina membranes obtained. Membranes with thicknesses of 0.5, 1.2, 50, 60, and 90 $\mu$m were prepared. The membranes were liberated by dissolving away the underlying (nonanodized) Al in a saturated aqueous solution of $HgCl_2$.

**Preparation of the Silica Nanotube Membranes.**[27−29] The first step in the protein biofunctionalization process involved reacting the membrane with an aldehyde silane. The aldehyde groups are then reacted by well-known Schiff-base chemistry to amine sites on the protein to be immobilized.[30,31] Hence, the quantity of protein that can be attached to the surface is determined by the extent of functionalization by the silane. In preliminary experiments on protein immobilization in such membranes, we found that higher levels of immobilization could be achieved if silica nanotubes were deposited within the pores prior to immobilization.[29] We investigated this issue quantitatively here by comparing the extent of silane functionalization for two different membrane systems—the commercial alumina nanopore membrane and the same membrane after deposition of silica nanotubes in the pores.[27−29] A sol−gel template synthesis method, described previously,[27,28] was used to deposit the silica nanotubes within the pores of the alumina membranes.

Briefly, the sol−gel silica precursor was prepared by mixing absolute ethanol, tetraethyl orthosilicate, and 1 M HCl (50:5:1 by volume). This solution was allowed to hydrolyze for 30 min. The alumina membrane was then immersed into this solution for 1 min under sonication. The sol-impregnated membrane was then dried in air for 10 min and oven-cured overnight at 150 °C. This yields silica nanotubes with wall thickness of ~3 nm[29] that line the pores of the alumina membrane. The surfaces of the membrane are also coated with silica, but these ultrathin (~3 nm) surface films do not block the mouths of the silica nanotubes.[29]

**Fluorescence-Based Method for Assaying the Extent of Silane Functionalization.** The as-prepared alumina and silica nanotube membranes were modified with the amino-terminated silane APTS. This was accomplished by immersing the samples into a solution that was 5% silane, 90% ethanol, and 5% acetate buffer (50 mM, pH 5.2). The beaker containing the solution and the immersed samples was placed in a vacuum chamber. A vacuum pump was used to pull a vacuum above the solution for 10 min to remove air from the pores or silica nanotubes. The membranes remained in this solution for another 20 min under ambient pressure. The APTS was then cured by heating in vacuum at 120 °C for 20 min. The same procedure was used to modify flat glass surfaces with APTS. Prior to functionalization, the glass slides were cleaned by immersion in piranha solution (a mixture of 3:1 (v/v) 98% $H_2SO_4$ and 30% $H_2O_2$) for 30 min. After rinsing


(23) Wu, Y.; de Kievit, P.; Vahlkamp, L.; Pijnenburg, D.; Smit, M.; Dankers, M.; Melchers, D.; Stax, M.; Boender, P. J.; Ingham, C.; Bastiaensen, N.; de Wijn, R.; van Alewijk, D.; van Damme, H.; Raap, A. K.; Chan, A. B.; van Beuningen, R. *Nucleic Acids Res.* **2004**, *32*, e123/121−e123/127.

(24) van Beuningen, R.; van Damme, H.; Boender, P. J.; Bastiaensen, N.; Chan, A. B.; Kievits, T. *Clin. Chem.* **2001**, *47*, 1931−1933.

(25) Masuda, H.; Satoh, M. *Jpn. J. Appl. Phys. 2* **1996**, *35*, L126−L129.

(26) Li, N.; Mitchell, D. T.; Lee, K.-P.; Martin, C. R. *J. Electrochem. Soc.* **2003**, *150*, A979−A984.

(27) Lakshmi, B. B.; Patrissi, C. J.; Martin, C. R. *Chem. Mater.* **1997**, *9*, 2544−2550.

(28) Brinker, C. J.; Scherer, G. W. *Sol−Gel Science*; Academic Press: New York, 1990.

(29) Lee, S. B.; Mitchell, D. T.; Trofin, L.; Nevanen, T. K.; Soederlund, H.; Martin, C. R. *Science* **2002**, *296*, 2198−2200.

(30) Bruning, C.; Grobe, J. *J. Chem. Soc., Chem. Commun.* **1995**, 2323−2324.

(31) Stubbings, D.; Bubb, M. O.; Conradie, J. D. *Anal. Biochem.* **1993**, *210*, 159−162.

with copious amounts of purified water and ethanol, the glass slides were blown dry with nitrogen and used immediately.

The amino group of APTS was then reacted with the isothiocyanate functionality of the fluorescent probe rhodamine B isothiocyanate.[32] This was accomplished by immersing the APTS-functionalized substrate (as-received alumina, silica nanotube membrane, or flat glass) into a 20 mM solution of the fluorescent probe (in dimethylformamide) for 16 h under nitrogen. The samples were then sonicated in dimethylformamide, chloroform, and ethanol (10 min in each solvent) and dried under nitrogen.

A fluorescence microscopy system was used to measure the fluorescence intensity from these samples and to obtain fluorescence and bright-field optical images of the arrays. This system combines an Axioplan 2 imaging microscope (Zeiss) with a J&M-PMT photometry system detector (SpectrAlliance), for measuring fluorescence intensity. In addition, the system is equipped with a digital CCD camera (Zeiss) to obtain both fluorescence and optical images. The excitation source for all fluorescence measurements was a mercury lamp. A beam splitter was used to send the reflected fluorescent light from the sample to the detector and the CCD camera. The rhodamine B was excited at 570 nm, and the emission was collected through a 590-nm band-pass filter.

**Fabrication of the Microarrays.** Figure 1 shows a schematic representation of the fabrication procedure. First, a thin (~90 nm) Au/Pd film was sputtered on one face of the commercial nanopore alumina membrane using a Desk II Cold Sputter instrument (Denton Vacuum, LLC). The Ar pressure was 75 mTorr, the sputtering current was 45 mA, and the sputtering time was 180 s. A copper TEM grid with 26-$\mu$m-diameter wires and 38-$\mu$m square holes between the wires was placed on top of the Au/Pd film (Figure 1A). This assembly was exposed to an Ar plasma (Samco Plasma Ion Etching System, model RIE-1C) for 10 min to etch away the Au/Pd adjacent to the holes in the grid but not beneath the wires in the grid (Figure 1B). The Ar plasma parameters were as follows: 13.56 MHz, 140 W, 10 Pa Ar, and Ar flow rate 12 sccm.

The square portions of membrane where the Au/Pd film was removed become the individual wells of the microarray. The Au/Pd-coated surfaces surrounding the wells were coated with Ag by using the Au/Pd as a cathode for electrochemical Ag plating. Electrical contact was made to the membrane by applying a piece of a conductive copper adhesive tape to the Au/Pd-coated surfaces surrounding the wells. Electroplating was accomplished using an EG&G PAR model 273 galvanostat/potentiostat controlled by a PC running the CorrWare software package (Scribner Associates, Inc.). A Teflon electrochemical cell (17-mm inner diameter) was used. The Ag was deposited galvanostatically using a Ag wire counter electrode.

Ag was deposited in two steps. In the first step, the Au/Pd-coated surface of the membrane faced up in the electrochemical cell, which primarily resulted in coating the Au/Pd with a thin (1 $\mu$m) layer of Ag (Figure 1C). The Ag was deposited at $-2$ mA cm$^{-2}$ for 8 min. The cell was then disassembled, and a film of the cresol Novolak FSC-M polymer was spun-coated over the face of the membrane that was coated with Ag (Figure 1D). This polymer film was ~3.5 $\mu$m thick and blocked all the pore openings at this surface of the membrane.

(32) Haugland, R. P. *Handbook of Fluorescent Probes and Research Products*, 9th ed.; Molecular Probes: Eugene, OR, 2002.

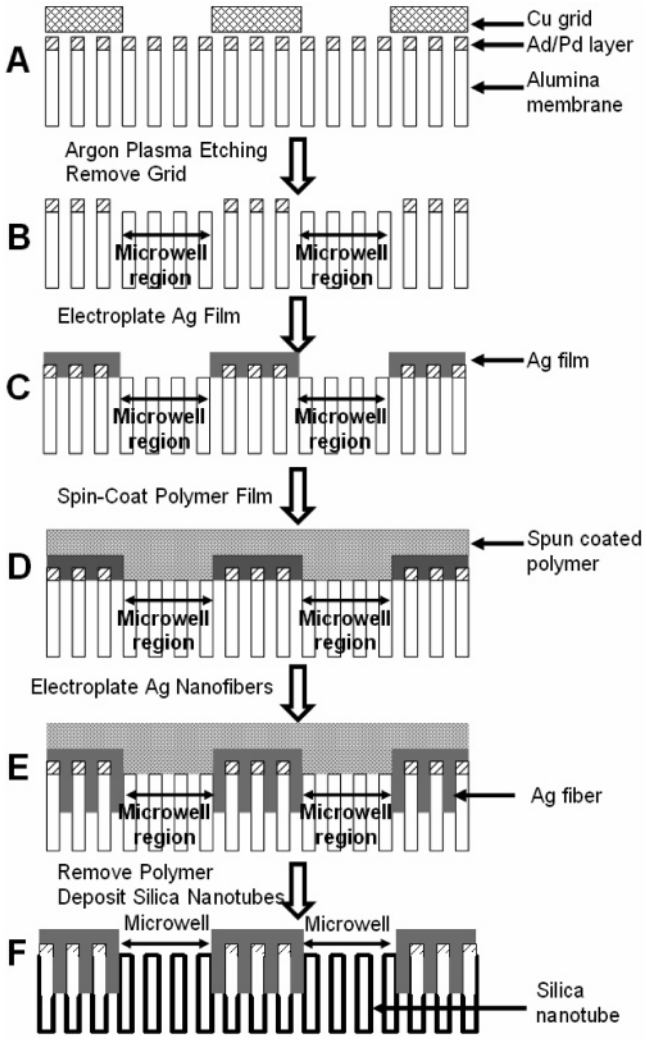


**Figure 1.** Schematic of the method used to prepare the microwell arrays. See text for details.

The membrane was then place into the electrochemical cell with the spun-coated film facing down and the open-pore surface facing up, and Ag was deposited at $-0.50$ mA cm$^{-2}$ for 90 min. Because the open-pore surface faced up, this Ag was deposited as nanofibers within the pores (Figure 1E). These nanofibers were deposited to make the membrane have greater mechanical strength. However, as shown in Figure 1E, Ag nanofibers were not deposited in the pores of the microwell regions. The polymer film was then removed using the Shipley 1165 solvent system, and silica nanotubes were deposited within the pores to yield the completed microwell array (Figure 1F).

**IgG Biofunctionalization of the Silica Nanotubes in the Microwells.** The microwell array was immersed into an ethanolic solution that was 5% acetate buffer (pH 5.2) and 5% triethoxysilylbutyl aldehyde to attach the aldehyde functional group to the silica nanotubes. A microspotting/solution injection system was then used to apply a solution of either human or mouse IgG to selected microwells in the array. Primary amines on the protein react with the aldehyde groups thus covalently attaching the protein to the nanotube walls.[30,31]

To accomplish this, the aldehyde-functionalized microwell array was placed on the stage of a Nikon microscope (10× lens, Part No. 19929) equipped with a Sony video camera whose signal was

fed to a display monitor. The feed tube of the microinjection system (Eppendorf FemtoJet, Fisher Scientific, Part No. 920010504) was clipped to the micromanipulator (Part No. 572), and this assembly was placed over the microwell array. The micromanipulator was used to position the Femtotip of the microinjection system into the desired microwell, and solution was dispensed until the entire surface within the microwell was covered with solution. The tip was then retracted, and the solution spontaneously wicked into the silica nanotubes within the microwell. The IgG solutions contained 0.2 mg of protein/mL and were prepared in phosphate-buffered saline, pH 7.4.

After application of protein solution into the desired microwells in the array, the array was immersed into the phosphate-buffered saline solution and incubated for 12 h at 4 °C. The arrays were then immersed for 3 h into a blocking solution that was 1% bovine serum albumin (BSA) and 0.1% Tween-20 dissolved in the phosphate-buffered saline. The BSA consumed any unreacted aldehyde groups and also blocked sites that would otherwise be available for nonspecific protein adsorption.[3,10]

After thorough washing, the arrays were incubated for 12 h in a solution that was 0.1 mg/mL both anti-human IgG and anti-mouse IgG prepared in the phosphate-buffered saline. The anti-human IgG was labeled with the fluorophore Alexa 488 and the anti-mouse IgG with the fluorophore Alexa 594. Fluorescence microscopy images were then obtained. Alexa 594 was excited at 570 nm, and the emission was detected through a 590-nm band-pass filter. The Alexa 488 was excited at 495 nm, and the emission was detected through a 515-nm band-pass filter. The fluorescent images were analyzed with Image Tool software (U. Texas Health Science Center).

**Scanning Electron Microscopy (SEM).** SEM was used to measure the pore diameter, pore density, and thickness of the alumina membranes and to image the completed microwell arrays. Images were obtained using a Hitachi S4000 FE-SEM. The pore diameter and pore density were calculated by analyzing the SEM images with the WSxM image analysis package (Nanotec Electronica). To improve the quality of the SEM image, the surface of the sample was sputtered with an ultrathin Au/Pd film prior to imaging.

## RESULTS AND DISCUSSION

**Assaying the Extent of Silane Functionalization.** As noted above, the first step in the protein biofunctionalization process involves reacting the membrane with a silane which is subsequently reacted with the protein. We investigated two different membrane systems—the commercial alumina nanopore membrane and the same membrane after deposition of silica nanotubes in the pores[28,29]—to determine which provided the highest extent of silane functionalization. The silane used for these studies was APTS.[3] The amino groups were then reacted with rhodamine B isothiocyanate to attach this fluorescent probe to the nanopore or nanotube walls.

The rhodamine B fluorescence signal from the silica nanotube membrane is ~7 times higher than from the alumina membrane (Figure 2). This result is consistent with previous studies that showed that the density of hydroxyl groups is higher on sol−gel silica surfaces (4−10 OH groups/nm$^2$) than on alumina surfaces (0.1−2.5 OH groups/nm$^2$).[33,34] Because the silica nanotube membranes showed higher silane-binding capacity, all subsequent studies were done with this membrane.

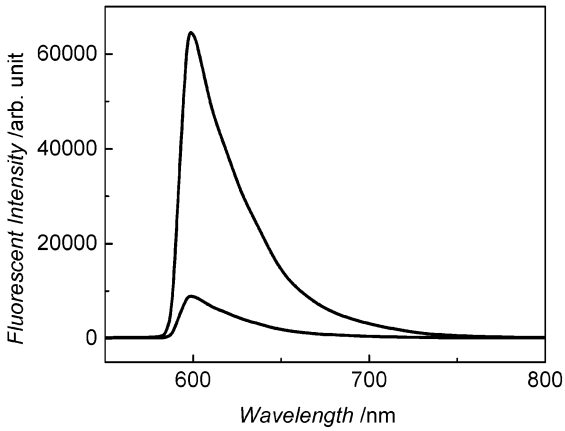


**Figure 2.** Rhodamine B fluorescence spectra from a nanopore alumina membrane (lower curve) and from an analogous membrane but with silica nanotubes deposited within the pores (upper curve).

**Effect of Membrane Thickness on Fluorescence Intensity.** A primary objective of this research effort was to demonstrate the advantages offered by this 3-D protein microarray relative to the more conventional 2-D array. The key advantage is that more analyte can be bound per square centimeter of array surface in the 3-D array.[4,13,23,24,35] This is because the analyte is deposited within the pore structure of the 3-D system as opposed to being simply deposited on the flat surface of the 2-D system. To demonstrate this advantage for our arrays, nanopore alumina membranes with thicknesses ranging from 0.5 to 90 $\mu$m were prepared, silica nanotubes were deposited within the pores, and rhodamine B was attached to the nanotube walls. The alumina membranes all had 72 ± 6 nm diameter pores and a pore density is $1.1 \times 10^{10}$ pores cm$^{-2}$.

Figure 3 shows rhodamine B fluorescence spectra from nanotube membranes with the indicated thicknesses. As anticipated, fluorescence intensity increases with membrane thickness, and even our thinnest nanotube membrane (0.5 $\mu$m) shows substantially higher fluorescence intensity than a rhodamine B-functionalized flat glass surface (inset Figure 3). These data were quantified by dividing the intensity from each nanotube membrane by the intensity from the flat glass surface. Figure 4 shows that this intensity ratio (left-hand *y*-axis) increases linearly with membrane thickness. The intensity ratios are the data points in this figure. The intensity from the thickest membrane is over 1000 times higher than from the flat glass surface. To our knowledge, this is by far the greatest enhancement of binding capacity and fluorescence signal observed for any 3-D array system.[4,6,11,16−19] These results suggest that array sensors based on our 3-D nanotube system will provide a very broad dynamic range of detection, which is especially useful for protein microarrays.

The available surface area for silane immobilization within each nanotube membrane can be calculated from the tube diameter,

(33) Tundo, P.; Venturello, P.; Angeletti, E. *J. Am. Chem. Soc.* **1982**, *104*, 6551−6555.
(34) Van der Voort, P.; Gillis-D'Hamers, I.; Vansant, E. F. *J. Chem. Soc., Faraday Trans.* **1990**, *86*, 3751−3755.
(35) Zhu, H.; Bilgin, M.; Bangham, R.; Hall, D.; Casamayor, A.; Bertone, P.; Lan, N.; Jansen, R.; Bidlingmaier, S.; Houfek, T.; Mitchell, T.; Miller, P.; Dean, R. A.; Gerstein, M.; Snyder, M. *Science* **2001**, *293*, 2101−2105.

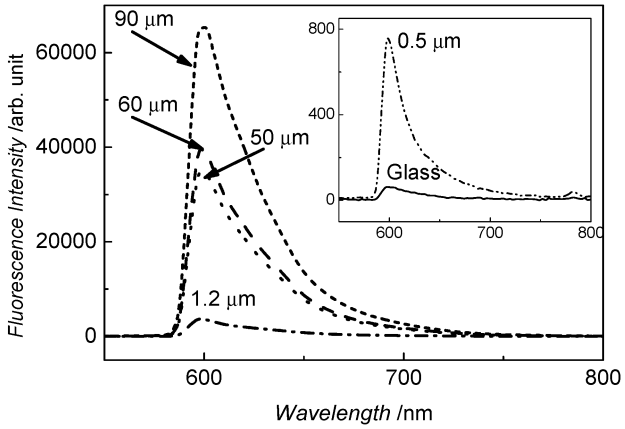


**Figure 3.** Rhodamine B fluorescence spectra from silica nanotube membranes with the indicated thicknesses. Inset compares the fluorescence spectra from the thinnest silica nanotube membrane and a flat glass surface.

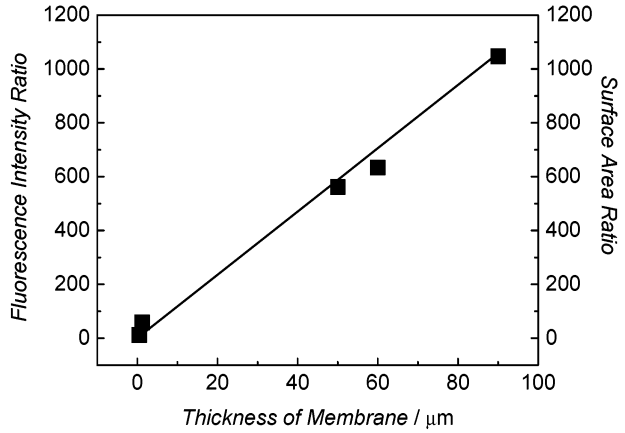


**Figure 4.** Experimental fluorescence intensity ratios (data points) (left-hand *y*-axis) plotted versus membrane thickness. The line is the surface area ratio (right-hand *y*-axis) calculated from the pore diameter, pore density, and membrane thickness plotted versus the thickness of the membrane.

pore density, and membrane thickness. Figure 4 shows that this surface/area ratio (right-hand *y*-axis) increases linearly with membrane thickness (solid line). This linear increase in available surface area explains why fluorescence intensity increases linearly with membrane thickness.

**Protein Microwell Arrays.** Scanning electron micrographs of the array surface clearly show the microwell regions (recessed) and the Ag film surrounding the microwells (Figure 5A). That the pores within the microwell regions are open at the membrane surface is shown by the micrograph in Figure 5B. It is important to point out that a number of procedures for creating array patterns in nanopore pore alumina membranes like those used here have recently been described.[36−42] None of these used silica nanotubes, and we have clearly demonstrated the advantage of the silica nanotube system in Figure 2. Furthermore, by depositing Ag nanofibers into the pores surrounding the mircowell regions of our arrays (Figure 1E and F), we dramatically improve the mechanical properties of the array. For example, our arrays can be cut with scissors, whereas alumina membranes without the Ag nanofibers are too brittle to be processed in this way. However, as will be discussed below, the most important advantage of our micropatterning method is that the Ag film surrounding the microwell regions (Figure 5A) show lower background fluorescence intensity than an alumina nanopore membrane surface that is not coated with Ag.

Figure 6A shows a bright-field optical image of the microwell array surface. The halogen lamp used to obtain this image was positioned below the sample, and the microwell regions contain the open silica nanotubes. This, and the fact that the alumina is translucent, causes the microwells to appear as bright squares in the image. Light cannot, however, propagate through the surrounding Ag regions, and so these appear black in the image (Figure 6A). The width of the microwells, and the distance between the wells, are 38 and 64 $\mu$m, respectively, which are identical to the dimensions of the TEM grid mask. The microwell density obtained from images such as Figure 6A is $2.4 \times 10^4$ wells $cm^{-2}$.

To demonstrate that this device can be used as a protein microarray, human IgG and mouse IgG were spotted in the pattern shown in Figure 6A. (It is important to recall that after spotting of the indicated microwells with IgG, the microwells that were not spotted were blocked by reaction with BSA.) The array was then exposed to a solution containing Alexa 488-tagged anti-human IgG (green fluorescence) and Alexa 594-tagged anti-mouse IgG (red fluorescence). Figure 6B shows a fluorescence image of the microwell array after exposure to the anti-human and anti-mouse IgG. Green fluorescence was observed from the microwells that were spotted with human IgG, and red fluorescence was observed from the microwells that were spotted with mouse IgG.

Figure 7A shows a red fluorescence image of a patterned microwell array after exposure to the anti-mouse and anti-human IgGs. The red fluorescence intensity versus position along the indicated white line was measured (Figure 7B). As expected, the highest fluorescence intensity is observed from the microwells that were spotted with mouse IgG (far left and far right spots). The fluorescent intensity is not, however, constant across the microwell. This undoubtedly reflects inhomogeneous delivery of the mouse IgG to the microwell. Better fluorescence homogeneity should be possible if more sophisticated spotting technologies[3] are used.

The centermost microwell in Figure 7 was spotted with human IgG. While the red fluorescence intensity (anti-mouse IgG) is lower than that from the microwells that were spotted with mouse IgG, the intensity is higher than from the microwells that were blocked with BSA (Figure 7B). This indicates that there is some cross-reactivity between the spotted IgGs; i.e., the human IgG in the center microwell has some affinity for anti-mouse IgG.[12,43]

(36) Sun, Z.; Kim, H. K. *Appl. Phys. Lett.* **2002**, *81*, 3458−3460.
(37) Li, A.-P.; Muller, F.; Birner, A.; Nielsch, K.; Gosele, U. *Adv. Mater.* **1999**, *11*, 483−487.
(38) Bae, E. J.; Choi, W. B.; Jeong, K. S.; Chu, J. U.; Park, G.-S.; Song, S.; Yoo, I. K. *Adv. Mater.* **2002**, *14*, 277−279.
(39) Lazarouk, S.; Katsouba, S.; Demianovich, A.; Stanovski, V.; Voitech, S.; Vysotski, V.; Ponomar, V. *Solid State Electron.* **2000**, *44*, 815−818.
(40) Yan, J.; Rama Rao, G. V.; Barela, M.; Brevnov, D. A.; Jiang, Y.; Xu, H.; Lopez, G. P.; Atanassov, P. B. *Adv. Mater.* **2003**, *15*, 2015−2018.
(41) Brevnov, D. A.; Barela, M.; Piyasena, M. E.; Lopez, G. P.; Atanassov, P. B. *Chem. Mater.* **2004**, *16*, 682−687.
(42) Liu, N.-W.; Datta, A.; Liu, C.-Y.; Peng, C.-Y.; Wang, H.-H.; Wang, Y.-L. *Adv. Mater.* **2005**, *17*, 222−225.
(43) Lueking, A.; Horn, M.; Eickhoff, H.; Bussow, K.; Lehrach, H.; Walter, G. *Anal. Biochem.* **1999**, *270*, 103−111.

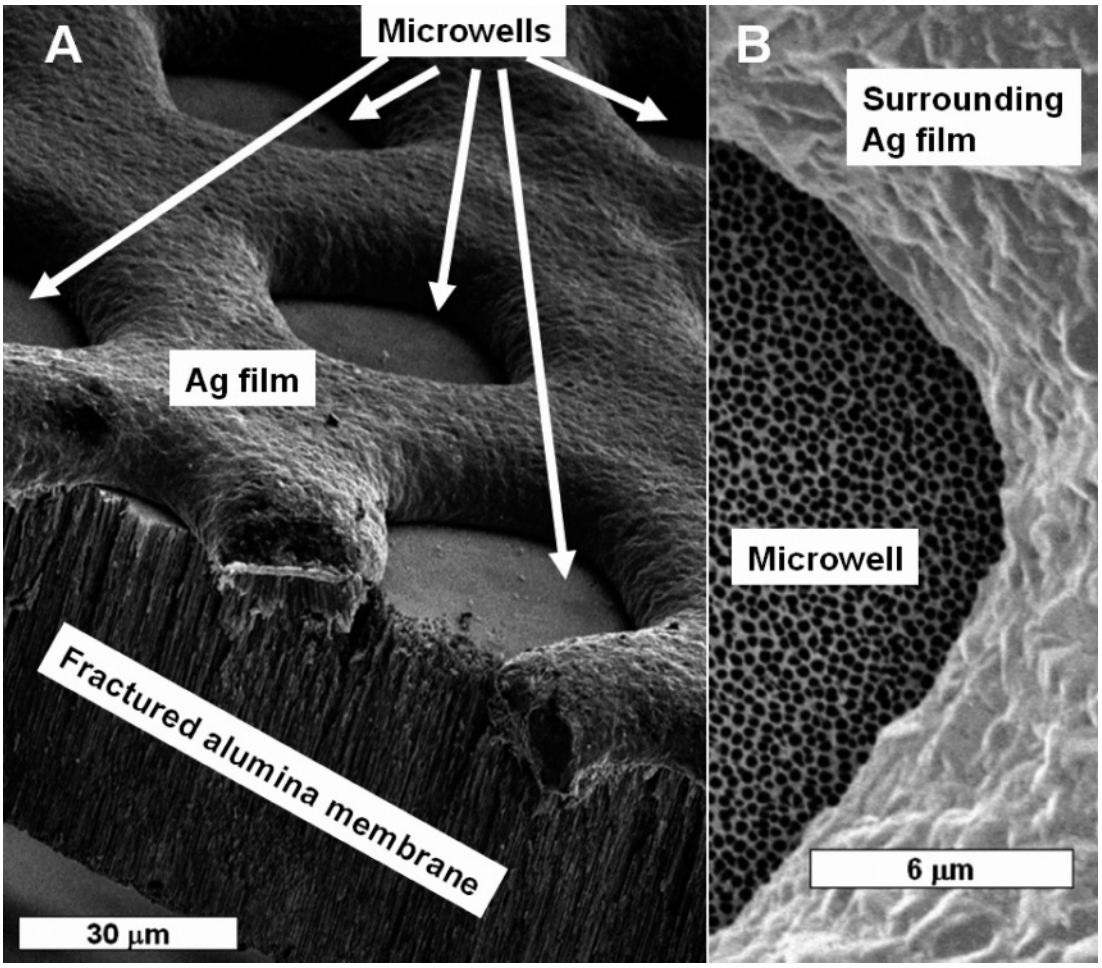


**Figure 5.** SEM images of the microwell array. (A) shows the fractured edge of the alumina membrane, the individual microwells, and the surrounding Ag film. (B) shows a closeup of the surface of a microwell and a portion of the surrounding Ag film.

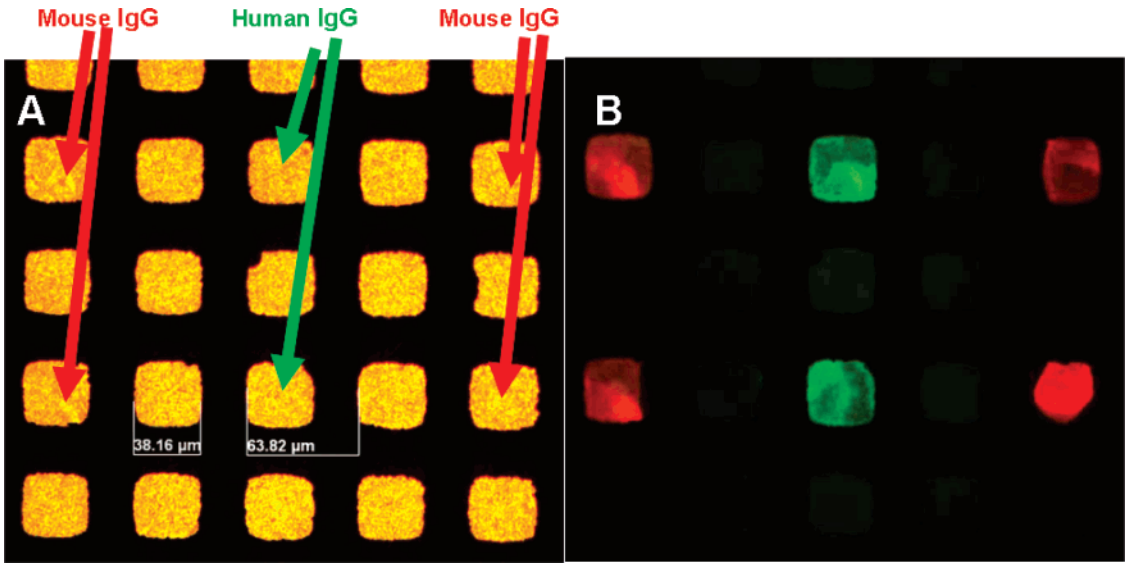


**Figure 6.** (A) Bright-field optical microscopic image of the microwell array. Mouse and human IgG were spotted as shown. (B) Fluorescence image of the microwell array in (A) after exposure to a solution containing Alexa 488-tagged anti-human IgG (green fluorescence) and Alexa 594-tagged anti-mouse IgG- (red fluorescence). The green and red fluorescence images are overlaid in this figure.

While much lower intensity was observed from the BSA-blocked microwells, the intensity was not zero. This indicates that some nonspecific adsorption of the anti-mouse IgG occurs despite the blocking BSA.

The final point to make concerns the very low fluorescence intensity observed from the regions of the array that were coated with Ag (labeled Ag in Figure 7B). The intensity from the Ag surfaces is 1 order of magnitude lower than from the BSA-blocked

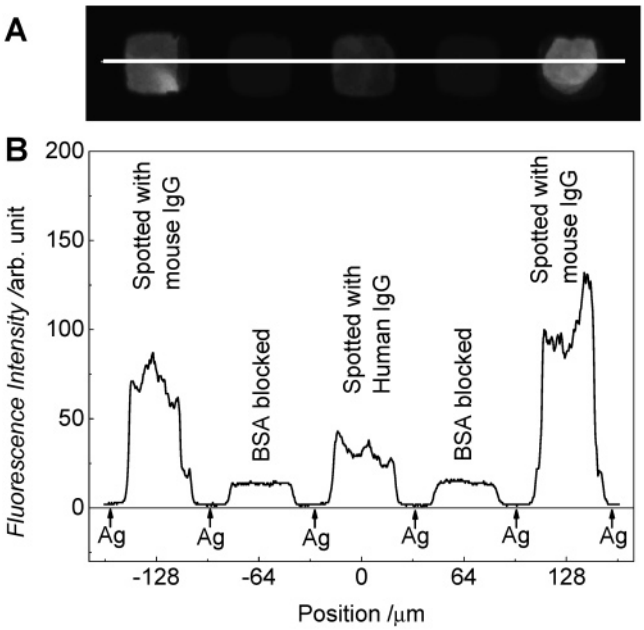


**Figure 7.** (A) Fluorescence microscopy image of a portion of a microwell array in which the elements contained (from left to right) mouse IgG, no IgG, human IgG, no IgG, and mouse IgG. The fluorescence is due to Alexa 594-tagged anti-mouse IgG. (B) Fluorescence intensity along the white line shown in (A).

microwells. As a result, the signal-to-background ratio for this array is better than for alumina membrane-based arrays[23,24] that do not have Ag borders around the microwells. Low fluorescence intensity is observed from the Ag because sites for nonspecific adsorption of the fluorescent anti-IgGs (mouse or human) were also blocked by the exposure to BSA. Furthermore, the Ag films are 2-D, and our studies with flat glass surfaces showed that fluorescence intensity from a flat surface is lower than from the 3-D nanopore surface. Finally, it is well known that metal films are very efficient fluorescence quenchers.[44]

(44) Lakowicz, J. R. *Principles of Fluorescence Spectroscopy*, 2nd ed.; Kluwer Academic/Plenum: New York, 1999.

## CONCLUSIONS

We have described a new approach for preparing platforms for array-based biosensors. This platform consists of 3-D nanotube-based microwells surrounded by metallic Ag borders (Figure 5). The dimensions of the microwells and the spacing between wells are determined by the characteristics of the TEM grid used as the mask to prepare the array, and grids with various wire sizes and spacing are available. Because the microwells are based on a nanopore membrane, analyte species are immobilized in three dimensions within the wells. This 3-D character provides arrays with binding capacities that can be 3 orders of magnitude higher than that of a flat glass surface (Figure 4), the most commonly used material in microarray technology. In addition, as has been demonstrated by Wu et al. for a different type of 3-D array, the porous structure will allow the array to be operated in a flow-through fashion, which improves both the speed and sensitivity of the assay.[23]

The metallic Ag surrounding the microwells shows very low fluorescence intensity, and this results in arrays that have excellent signal-to-background ratios (Figure 7B). In addition, the Ag borders between the microwells minimize the risk of cross contamination of the microwells during spotting. The Ag nanofibers deposited within the pores beneath the Ag film provide enhanced mechanical strength relative to arrays based on the alumina membrane alone. Metals other than Ag could also be employed.

## ACKNOWLEDGMENT

This work was supported by the National Science Foundation.

Received for review May 20, 2005. Accepted July 27, 2005.

AC0508907